Journal Pre-proofs

Analytical solution of the cantilevered elastica subjected to a normal, uniformly distributed follower load

Ettore Barbieri

PII: S0020-7683(20)30253-5
DOI: https://doi.org/10.1016/j.ijsolstr.2020.06.031
Reference: SAS 10769

To appear in: *International Journal of Solids and Structures*

Received Date: 14 March 2020
Accepted Date: 23 June 2020

Please cite this article as: E. Barbieri, Analytical solution of the cantilevered elastica subjected to a normal, uniformly distributed follower load, *International Journal of Solids and Structures* (2020), doi: https://doi.org/10.1016/j.ijsolstr.2020.06.031

Analytical solution of the cantilevered elastica subjected to a normal, uniformly distributed follower load

Ettore Barbieri[a,*]

[a]Japan Agency for Marine-Earth Science and Technology (JAMSTEC)
Center for Mathematical Science and Advanced Technology (MAT)
Yokohama Institute for Earth Sciences (YES)
3173-25, Showa-machi, Kanazawa-ku, Yokohama-city, Kanagawa, 236-0001, Japan

Abstract

We report the full analytical solution of the large deformations of a cantilevered elastica loaded by a uniformly distributed follower pressure. We consider an unshearable, inextensible and linear elastic rod. We obtain a spatial nonlinear differential equation in the curvatures, analogous to the undamped Duffing oscillator with a constant driving force. We solve such differential equation, obtaining the curvature, although in implicit form, for arbitrarily large values of the load. We are then able to obtain the rotations owing to a change of variables from the curvilinear abscissa to the curvature. This step is somewhat mandatory due to the implicit nature of the solution. Finally, with the same change of variables, it is possible to obtain a closed-form solution for the deformation in Cartesian coordinates. The solutions show that the rod deforms into drop-like shapes. The number of drops is equal to the number of spatial periods of the solution, which goes with $q^{*1/3}$, with q^* a dimensionless load normalised to the bending stiffness. Interestingly, we find that for $q^* \geq 3094.2$, the number of drop-like shapes does not increase, but remains three.

Keywords: elastica, follower, analytical, Duffing, pressure, cantilever

1. Introduction

The cantilevered beam is arguably the most common and iconic structure in the mechanics of solids. Euler's Elastica theory, an equally famous and well-studied set of differential equations, describes the large deformations of the beam. A collection of solutions of the elastica under terminal loads (shear or axial forces) and distributed loads with a fixed direction can be found in several monographs Bigoni (2012); Frisch-Fay (1962); Antman (1995); Manning (2014).

In contrast to loads with a fixed direction, follower loads change their direction according to the deformation. For example, normal follower loads like hydrostatic pressure remain perpendicular to the deformation.

*Corresponding author
Email address: e.barbieri@jamstec.go.jp (Ettore Barbieri)

Early theoretical research on follower forces focused instead on tangential follower forces. The most famous works include the Pflüger column Pflüger (1950, 1955); Tommasini et al. (2016); Bigoni et al. (2018b), the Ziegler paradox Ziegler (1952, 1956); Bottema (1956); Ziegler (1977); Bigoni et al. (2018a), the Beck's column Beck (1952), the Reut's column problem Reut (1939); Bigoni and Misseroni (2020), and the first monograph on the stability of non-conservative forces due to Bolotin (1963).

Other researchers attempted to realise follower forces experimentally. Herrmann et al. (1966) and Wood et al. (1969) used water and air flowing from a nozzle; Sugiyama et al. (1995, 1999, 2000) used a solid motor rocket instead. However, as Elishakoff pointed out in 2005 Elishakoff (2005), none of these methods correctly realised a tangential follower force because of hydrodynamical effects influencing the motion of the rod and in non-negligible and variable mass of the rocket. A significant breakthrough was achieved in 2011 by Bigoni and Noselli Bigoni and Noselli (2011), who designed and tested a device capable of realising a follower tangential force emerging at the contact with the friction of a wheel constrained to slide against a moving surface.

Theoretical studies regarding normal follower forces include Batista (2014), where he obtained an analytical solution of the elastica under a terminal shear follower force. For distributed normal follower loads, a considerable body of literature exists on the elasticity of closed curves under hydrostatic pressure. Such problem attracted the curiosity of numerous theoreticians since 1884 Lévy (1884); Greenhill (1899). In a more modern perspective, numerous researchers Djondjorov et al. (2011); Giomi (2013); Vassilev et al. (2008); Giomi and Mahadevan (2012); Mora et al. (2012) interested in the equilibrium shapes of films under surface tension revisited the problem of a ring under hydrostatic pressure.

Recently, Salussolia et al. (2020) studied the liquid-phase exfoliation of graphite sheets as a scalable manufacturing method for the mass production of graphene. The fluid exerts resultant loads on a delaminated sheet that, in addition to a terminal follower force, include a follower distributed load. In this case, as in most peeling problems, the cantilevered beam is an idealisation of the graphite. Therefore, there seems to be a renewed interest in the cantilevered elastica under a distributed uniform follower load, fostered by the need of manufacturing advanced materials.

However, it is a problem that seems to have been overlooked in the literature. The elastica with terminal loads usually admits a closed-form solution in terms of Jacobi elliptic functions. Distributed loads, either fixed or follower, complicate the governing equations considerably. Of course, numerical solutions exist for this problem. Fujii et al. (1990) used a field transfer matrix to obtain the force-displacement curve of a cantilever beam subjected to water pressure. Faulkner et al. (1993) used the segmental shooting technique, which divides the elastica in a sequence of segments, each subjected to small deformations. They obtained the deformation for normal loaded cantilevers.

Regarding analytical treatments, Truesdell (1953) derived a polar inertia method for the free shape problem of a given deformation of the elastica under a normal and uniform follower pressure. He was able

to obtain an expression between the curvature of the free shape and the curvature and the chord of the assigned shape. For the rotation, this relation turns out to involve the integral of the square of the chord. This integral is then the polar moment of inertia of the bar with respect to an axis perpendicular to the plane of the deformation and passing through the free end.

Mitchell (1959) obtained an implicit solution in polar coordinates for the cantilevered elastica under uniform follower load. The starting point of the solution appears to be the moment-curvature relation, rather than the equilibrium equations. Contrarily to Mitchell (1959), we start from the equations of equilibrium of axial and normal forces and moments. Conversely from Mitchell (1959), it turns out that the differential equation for the curvatures is solvable independently from the rotation and the deformation.

We show in this paper that the follower elastica with a uniform load leads to a famous and approachable second-order nonlinear differential equation. Indeed, the curvatures follow a variant of the well-known Duffing equation. Such differential equation emerged mutatis mutandis also in Djondjorov et al. (2011) and Giomi (2013). However, differently from Djondjorov et al. (2011); Giomi (2013), in this paper, we do not consider closed curves; we study, instead, an open curve, cantilevered at one end and free at the opposite end as in figure 1. This difference brings some obstacles in obtaining the solution, starting from the fact that the Jacobi elliptic functions do not help. In fact, we will see that instead hypergeometric functions are more apt in describing the curvatures. Such special functions (or their modifications) were used for the elastica with dead loads also in Scarpello and Ritelli (2011) and Iandiorio and Salvini (2020).

We proceed as follows. We first solve the Duffing equation for the curvatures: we will see that the solution is periodic (in space) and given in an implicit form. For this reason, to integrate the curvature, we apply a crucial change of variables. Once the rotations are known, we integrate the cosine and sine of the rotation to obtain the deformations in Cartesian coordinates. Once again, the critical step is the change in the integration variables. Finally, we analyse the obtained shapes, and we find that with increasing amplitude of the load, the rod deforms into drop-like shapes. The maximum number of drops, however, is three. Beyond a specific load, that we quantify, the deformation appears to remain the same and rotate around the origin, although this is an optical illusion due to the self-contact that we do not enforce. The radius of the drops decreases with a power law with exponent $-1/3$ of the load.

2. Governing equations: the elastica with a follower load

The equations of equilibrium of forces and moments of a bent, elastic, unshearable and inextensible rod with a follower normal load q, as in figure 2, are Frisch-Fay (1962) , Antman (1968):

$$M'' - \kappa N - q = 0 \tag{1}$$

$$\kappa M' + N' = 0 \tag{2}$$

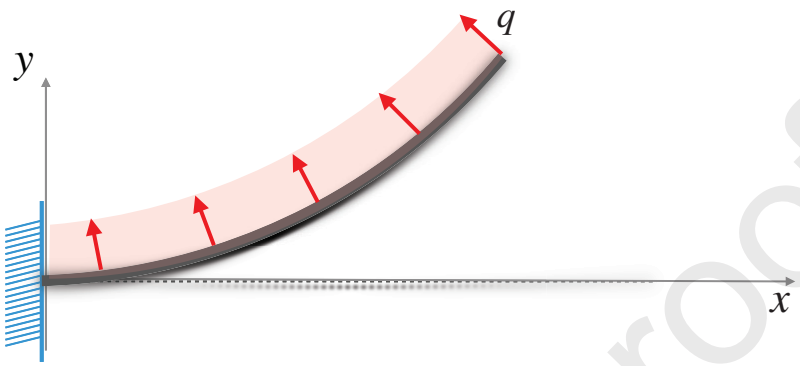

Figure 1: Cantilevered elastica loaded by a uniform follower load.

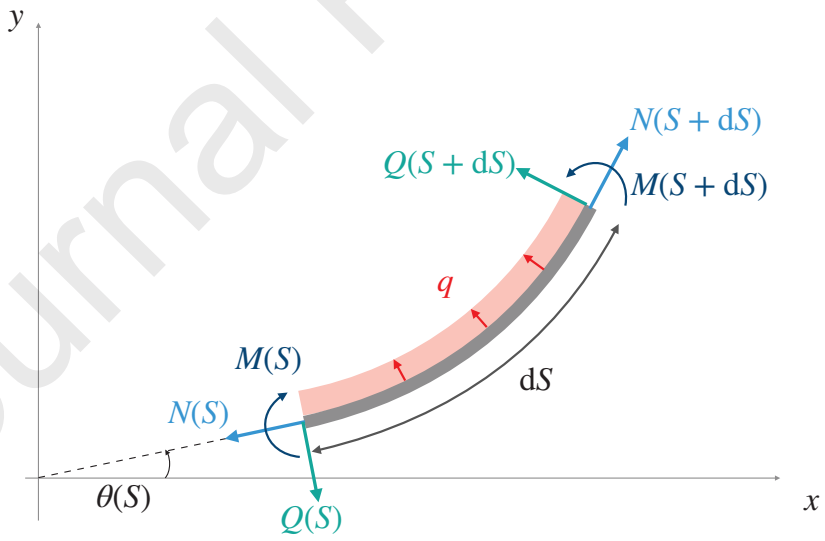

Figure 2: Free body diagram and sign convention.

where $(\cdot)' \equiv \mathrm{d}/\mathrm{d}S$, with S being the arc length, M is the bending moment and N is the axial force. The kinematics of the rod is given by

$$\kappa = \theta' \tag{3}$$

with κ the curvature, θ the rotation of the beam and

$$\begin{aligned} x' &= \cos\theta \\ y' &= \sin\theta \end{aligned} \tag{4}$$

with x and y the Cartesian components of the deformation.

In addition, we assume a homogeneous material and uniform cross-section along the whole beam with bending stiffness EI and moment-curvature relation

$$M = E\,I\,\kappa \tag{5}$$

Substituting the constitutive model (5) into equation (2), we get

$$N' = -EI\,\kappa\,\kappa' = -\left(E\,I\,\frac{\kappa^2}{2}\right)' \tag{6}$$

Integration of equation (6) between 0 and S gives

$$N(S) - N_0 = \frac{E\,I}{2}\,{\kappa_0}^2 - \frac{E\,I}{2}\kappa^2 = \frac{1}{2}\,M_0\,\kappa_0 - \frac{E\,I}{2}\kappa^2 \tag{7}$$

which can also be re-written as

$$N + \frac{E\,I}{2}\kappa^2 = \frac{1}{2}\,M_0\,\kappa_0 + N_0 \tag{8}$$

where N_0 is the axial force applied to the free end, M_0 the applied moment and κ_0 the curvature.

Substituting equation (7) and using the constitutive model (5) into equation (1), we get

$$E\,I\,\kappa'' - \kappa\left(N_0 + \frac{1}{2}\,M_0\,\kappa_0\right) + \frac{E\,I}{2}\kappa^3 - q = 0 \tag{9}$$

We now pass to the dimensionless form using

$$q^* = q\,L^3/E\,I, \qquad S^* = \frac{S}{L}\,\frac{1}{{S_{\max}}^*}, \qquad \kappa^* = \kappa\,L\,\frac{1}{{\kappa_{\max}}^*} \tag{10}$$

with L the length of the undeformed beam and

$${S_{\max}}^* = 2\,\alpha\,{q^*}^{-1/3}, \qquad \kappa^*_{\max} = 2\,{q^*}^{1/3}, \qquad \alpha = {}_2F_1\left(\frac{1}{6}, \frac{1}{2}; \frac{7}{6}; 1\right) \approx 1.214 \tag{11}$$

where ${}_2F_1\left(\frac{1}{6}, \frac{1}{2}; \frac{7}{6}; \cdot\right)$ is the hypergeometric function of parameters (1/6, 1/2) and 7/6. The variables ${S_{\max}}^*$ and ${\kappa_{\max}}^*$ are rescaling variables, so that $\kappa^* \leq 1$.

Indeed, despite the seemingly odd choice of scaling, equation (9) becomes

$$\kappa'' + 8\,\alpha^2\,\kappa^3 - 2\,\alpha^2 = 0 \tag{12}$$

where we have removed the * for ease of reading and used the boundary conditions $N_0 = M_0 = \kappa_0 = 0$. If we set the origin of the curvilinear abscissa at the free end, the remaining boundary conditions become

$$\begin{aligned}
&\kappa'(0) = 0 && \text{no applied shear force}\\
&\kappa(0) = 0 && \text{no applied moment}\\
&\theta(1/S^*_{\max}) = 0 && \text{cantilevered beam}\\
&x(1/S^*_{\max}) = 1/S^*_{\max} && \text{cantilevered beam}\\
&y(1/S^*_{\max}) = 0 && \text{cantilevered beam}
\end{aligned} \tag{13}$$

3. Analytical Solution

3.1. Phase portrait analysis

Let us multiply both sides of equation (12) by κ' and integrate between 0 and S. We obtain the following equation:

$$\kappa'^2 = 4\alpha^2\,\kappa\,(1 - \kappa^3) \tag{14}$$

which represents a closed path in the phase space $\kappa' - \kappa$; therefore, the solution is a periodic function (figure 3). Also, $\kappa' = 0$ when $\kappa = 0$ and $\kappa = 1$, and the curvatures $0 \le \kappa \le 1$.

Differentiating the implicit function in equation (14), we also find that

$$\kappa' \in [-\kappa'_{\max},\ \kappa'_{\max}], \qquad \kappa'_{\max} = 2^{-1/3}\,3^{1/2}\,\alpha \approx 1.6694 \qquad \text{when} \qquad \kappa = 2^{-2/3} \approx 0.63 \tag{15}$$

The solution proceeds anticlockwise from the initial condition $\kappa(0) = 0$ with initial slope $\kappa' = 0$ (figure 4). The solution then reaches a maximum for $S = 1$ where $\kappa' = 0$ and $\kappa = 1$; then, since $\kappa \ge 0$, the curvature decreases to $\kappa = 0$ and $\kappa' = 0$ and afterwards it repeats periodically with period equal to 2.

3.2. Solution for the curvatures

The equation (14) can be written as

$$\kappa'\ \operatorname{sign}\kappa' = 2\,\alpha\ \sqrt{\kappa}\ \sqrt{1 - \kappa^3} \tag{16}$$

or

$$\frac{1}{\alpha}\,\frac{\mathrm{d}\,\kappa}{2\ \sqrt{\kappa}\ \sqrt{1 - \kappa^3}}\ \operatorname{sign}\kappa' = \mathrm{d}S \tag{17}$$

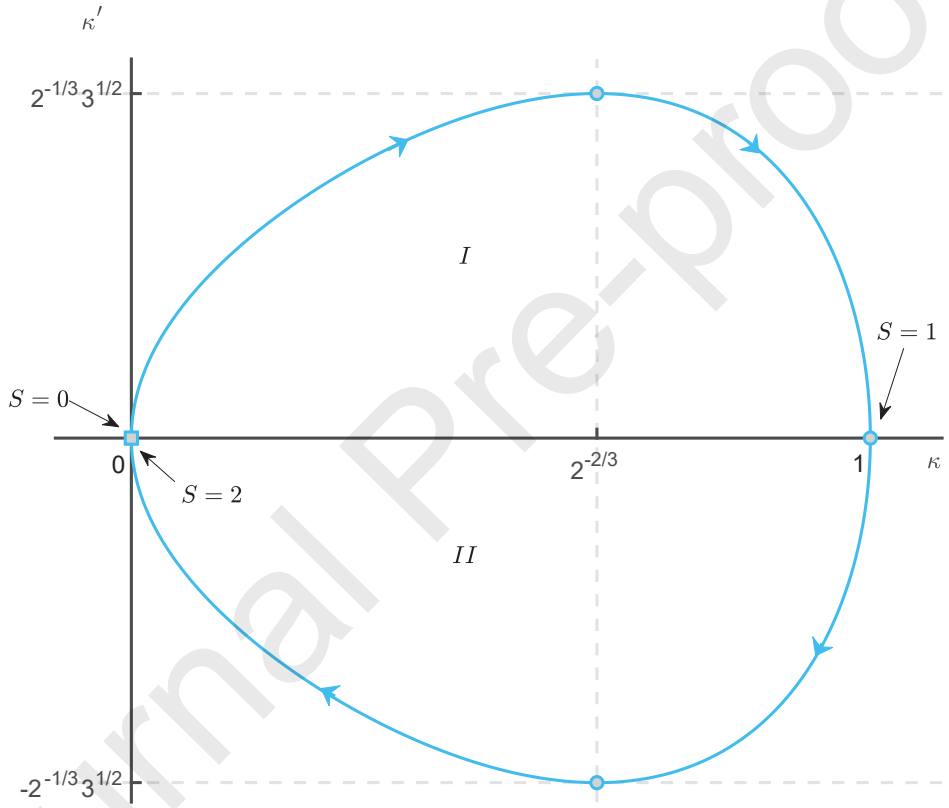

Figure 3: Phase portrait of equation (14).

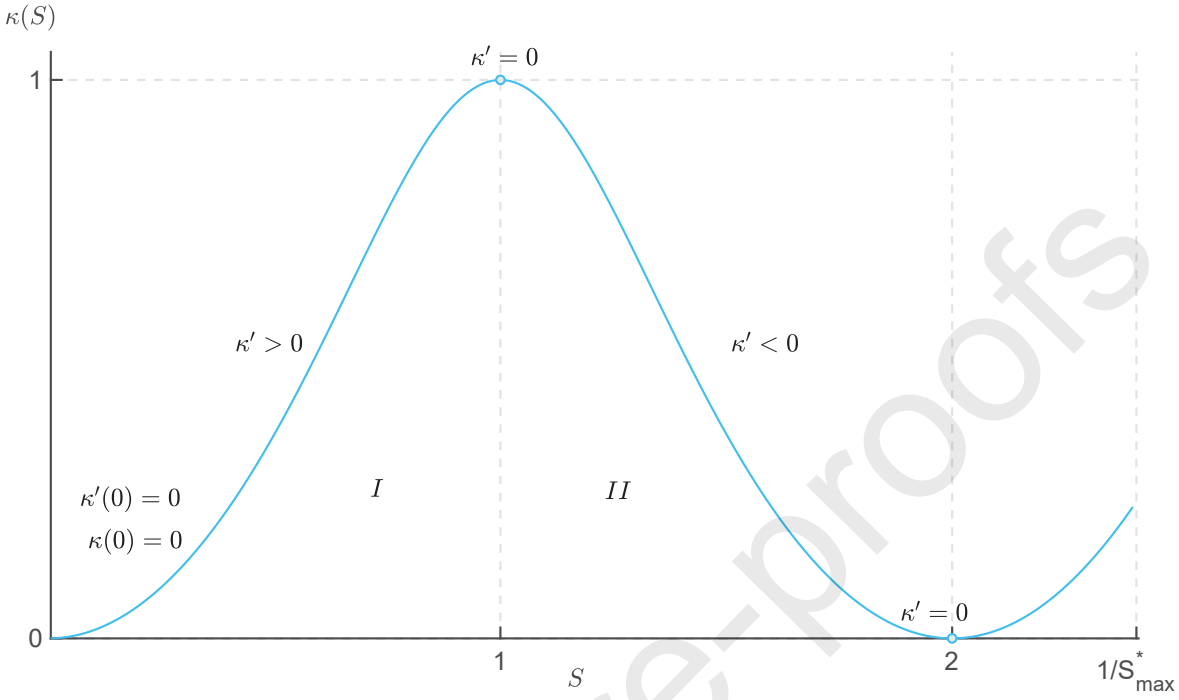

Figure 4: Solution $\kappa(S)$ for $S \in [0, 1/S^*_{\max}]$.

Let us introduce the following primitive (figure 5)

$$I(\kappa) = \frac{1}{2\,\alpha} \int_0^{\kappa} \frac{\mathrm{d}\,\kappa}{\sqrt{\kappa}\,\sqrt{1-\kappa^3}} = \frac{\sqrt{\kappa}\;{}_2F_1\left(\frac{1}{6}, \frac{1}{2}; \frac{7}{6}; \kappa^3\right)}{{}_2F_1\left(\frac{1}{6}, \frac{1}{2}; \frac{7}{6}; 1\right)} \tag{18}$$

that satisfies $I(0) = 0$ for $S = 0$ and $I(1) = 1$ at the half-period $S = 1$. We can integrate equation (16) by parts

$$I(\kappa)\ \mathrm{sign}\,\kappa' - \int_0^{\kappa} I(\kappa)\,\frac{\mathrm{d}\,\mathrm{sign}\,\kappa'}{\mathrm{d}\kappa} = S \tag{19}$$

The derivative of the sign of κ' with respect to κ is a sum of Dirac delta functions, centred at $\kappa = 0$ and $\kappa = 1$. There is a discontinuity for κ' at $\kappa = 1$ (sign changes from positive to negative) and at $\kappa = 0$ (sign changes from negative to positive).

$$\frac{\mathrm{d}\,\mathrm{sign}(\kappa')}{\mathrm{d}\kappa} = 2\sum -\delta(\kappa - 1) + \delta(\kappa) \tag{20}$$

Considering that $I(0) = 0$ and $I(1) = 1$, and that $\mathrm{sign}(x) = 1/\,\mathrm{sign}(x)$, we get

$$I(\kappa) = S\ \ \mathrm{sign}(\kappa') - 2\,n_{\downarrow}\ \mathrm{sign}(\kappa') \tag{21}$$

where $n_{\downarrow}$ is the number of times κ' changes sign from positive to negative between 0 and S.

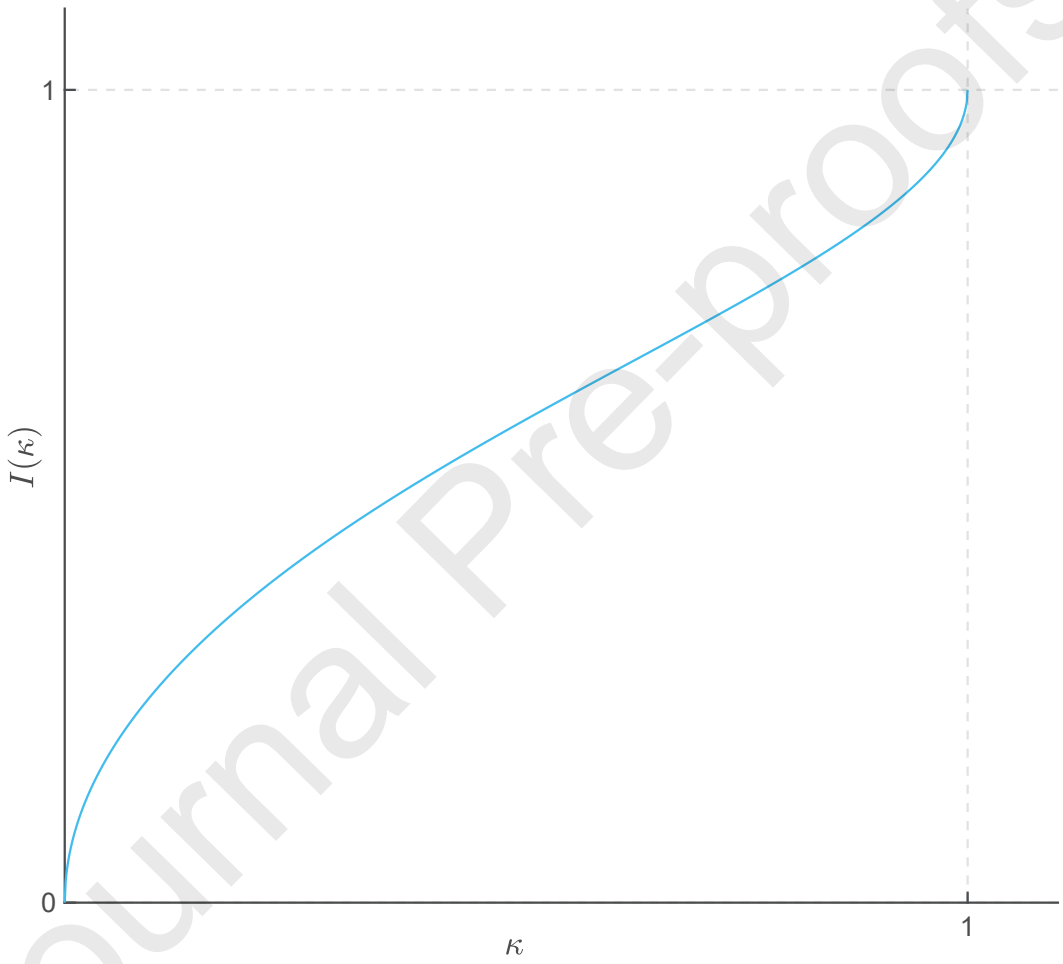

Figure 5: Function $I(\kappa)$ in equation (18).

Let us write equation (21) for the first intervals of S:

$$0 \le S \le 1: \qquad \mathrm{sign}(\kappa') = +1, \qquad n_\downarrow = 0, \qquad I(\kappa) = S \tag{22a}$$

$$1 < S \le 2: \qquad \mathrm{sign}(\kappa') = -1, \qquad n_\downarrow = 1, \qquad I(\kappa) = -S + 2 \tag{22b}$$

$$2 < S \le 3: \qquad \mathrm{sign}(\kappa') = +1, \qquad n_\downarrow = 1, \qquad I(\kappa) = S - 2 \tag{22c}$$

$$3 < S \le 4: \qquad \mathrm{sign}(\kappa') = -1, \qquad n_\downarrow = 2, \qquad I(\kappa) = -S + 4 \tag{22d}$$

All the intervals in equation (22) can be summarised into a single equation

$$I(\kappa) = T(S) \tag{23}$$

where $T(S)$ is the triangle wave shown in figure 6. The function $T(S)$ provides periodicity to the solution $\kappa(S)$ and takes into account the changes in sign of κ'. Many expressions exist for the triangle wave: we suggest the following surrogate expression:

$$T(S) = \frac{2}{\pi} \arcsin\left(\left| \sin\left(\frac{\pi}{2} S \right) \right| \right) \tag{24}$$

and using the differentiation rule for implicit functions

$$\mathrm{sign}\,(\kappa') = \mathrm{sign}\,(\sin(\pi S)) \tag{25}$$

In addition, an expression for $n_\downarrow(S)$ is

$$n_\downarrow(S) = 1 + \left\lfloor \frac{S-1}{2} \right\rfloor \tag{26}$$

where $\lfloor \cdot \rfloor$ is the floor function.

3.3. Solution for the rotations

With boundary condition $\theta(1) = 0$, the rotation is

$$\theta(S) = \beta(S) - \beta_1 \tag{27}$$

where

$$\beta(S) = 4\,\alpha \int_0^S \kappa(S)\,\mathrm{d}S, \qquad \beta_1 = \beta\left(\frac{1}{S_{\max}{}^*} \right) \tag{28}$$

We now use equation (17) to get

$$\beta(S) = 4\,\alpha \int_0^S \kappa(S)\,\mathrm{d}S = 2 \int_0^\kappa \frac{\sqrt{\kappa}}{\sqrt{1-\kappa^3}}\ \mathrm{sign}\,\kappa'\,\mathrm{d}\,\kappa \tag{29}$$

We can now integrate by parts with the same procedure used for equation (19), that is writing $\mathrm{d}\,\mathrm{sign}\,\kappa'/\mathrm{d}\kappa$ as a series of Dirac delta functions,

$$\beta(S) = \frac{4}{3} \arcsin \kappa^{3/2}\ \mathrm{sign}\,\kappa' + \frac{4}{3}\,\pi\, n_\downarrow(S) \tag{30}$$

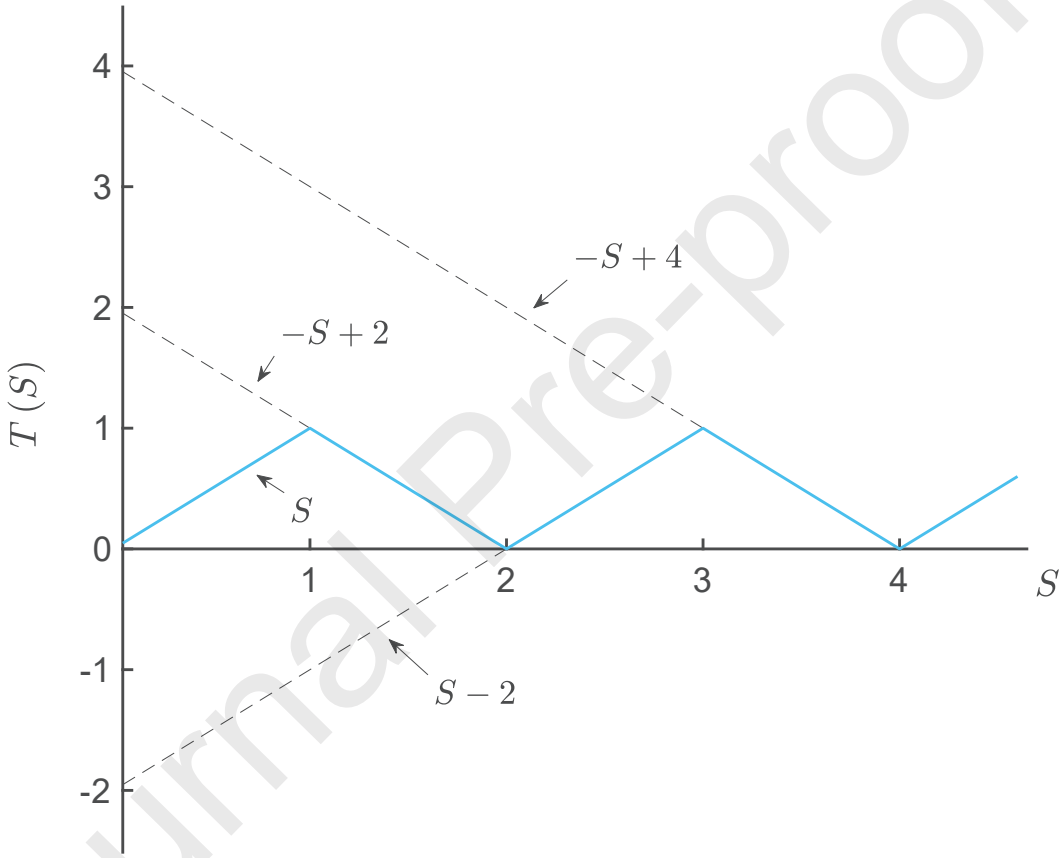

Figure 6: Function $T(S)$ (thick blue line) for the implicit solution of the nonlinear ODE is $I(\kappa) = T(S)$.

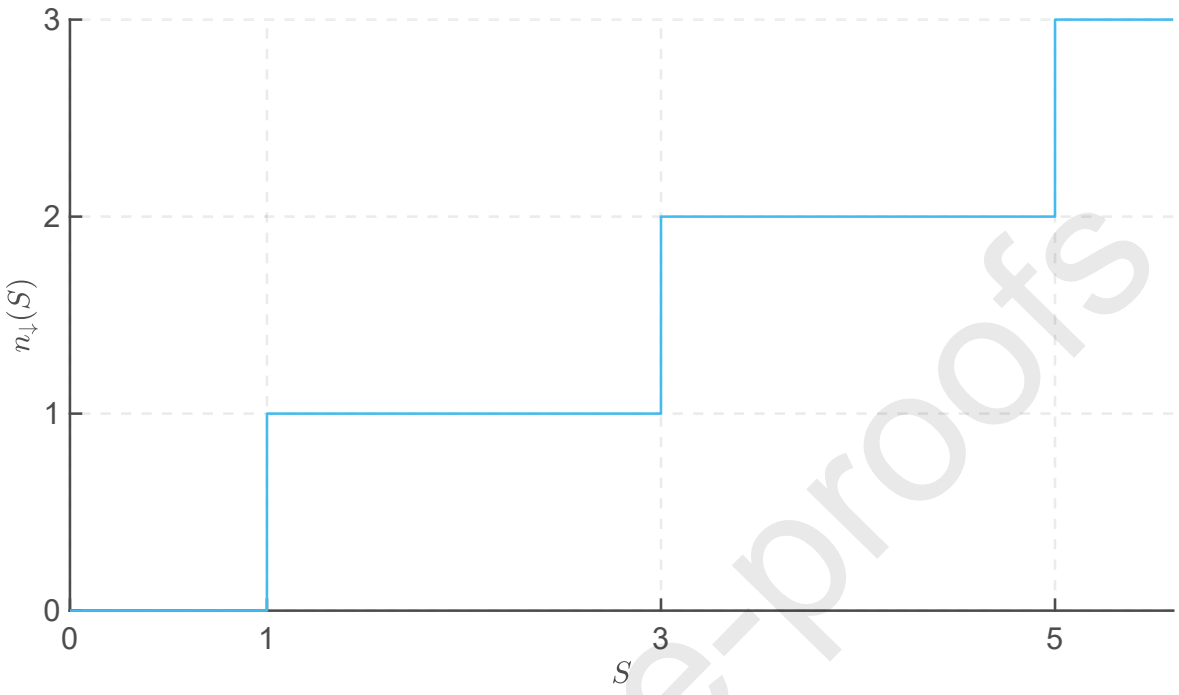

Figure 7: Function $n_{\downarrow}(S)$ in equation (26)

3.4. Solution for the deformation

With boundary condition (13), the dimensionless coordinates of the deformed configuration are given by

$$x(S) = \frac{1}{S_{\max}{}^*} - \int_1^S \cos\theta(S)\,\mathrm{d}S = \frac{1}{S_{\max}{}^*} - \int_0^1 \cos\theta(S)\,\mathrm{d}S + \int_0^S \cos\theta(S)\,\mathrm{d}S \tag{31a}$$

$$y(S) = -\int_1^S \sin\theta(S)\,\mathrm{d}S = -\int_0^1 \sin\theta(S)\,\mathrm{d}S + \int_0^S \sin\theta(S)\,\mathrm{d}S \tag{31b}$$

We notice that

$$\cos\theta = \cos\beta_1\cos\beta + \sin\beta_1\sin\beta \tag{32}$$

$$\sin\theta = \sin\beta_1\cos\beta - \cos\beta_1\sin\beta \tag{33}$$

where β_1 is the angle at the free tip. Therefore, let us shift the focus on the two integrals

$$\int_0^S \cos\beta(S)\,\mathrm{d}S = \frac{1}{2\,\alpha}\int_0^\kappa \frac{\cos\beta(\kappa)}{\sqrt{\kappa}\,\sqrt{1-\kappa^3}}\,\mathrm{sign}\,\kappa'\,\mathrm{d}\kappa \tag{34a}$$

$$\int_0^S \sin\beta(S)\,\mathrm{d}S = \frac{1}{2\,\alpha}\int_0^\kappa \frac{\sin\beta(\kappa)}{\sqrt{\kappa}\,\sqrt{1-\kappa^3}}\,\mathrm{sign}\,\kappa'\,\mathrm{d}\kappa \tag{34b}$$

In addition,

$$\cos\beta(S) = \cos\left(\frac{4}{3}\ \arcsin\kappa^{3/2}\ \operatorname{sign}\kappa' + \frac{4}{3}\pi\, n_{\downarrow}(S)\right) \tag{35a}$$

$$\sin\beta(S) = \sin\left(\frac{4}{3}\ \arcsin\kappa^{3/2}\ \operatorname{sign}\kappa' + \frac{4}{3}\pi\, n_{\downarrow}(S)\right) \tag{35b}$$

$$\tag{35c}$$

Considering that $\cos(x\ \operatorname{sign} x) = \cos x$ and $\sin(x\ \operatorname{sign} x) = \sin x\ \operatorname{sign} x$, we obtain the following integrand functions in (34a) and (34b):

$$C_c\,\frac{\cos\left(\frac{4}{3}\ \arcsin\kappa^{3/2}\right)}{\sqrt{\kappa}\ \sqrt{1-\kappa^3}} + \mathcal{S}_c\,\frac{\sin\left(\frac{4}{3}\ \arcsin\kappa^{3/2}\right)}{\sqrt{\kappa}\ \sqrt{1-\kappa^3}} \tag{36}$$

$$\mathcal{S}_s\,\frac{\cos\left(\frac{4}{3}\ \arcsin\kappa^{3/2}\right)}{\sqrt{\kappa}\ \sqrt{1-\kappa^3}} + C_s\,\frac{\sin\left(\frac{4}{3}\ \arcsin\kappa^{3/2}\right)}{\sqrt{\kappa}\ \sqrt{1-\kappa^3}} \tag{37}$$

where C_c, $\mathcal{S}_c$, $\mathcal{S}_s$ and C_s are piece-wise constant functions, with jumps at $i\,S_{\max}$, $i = 1, 3, 5, \ldots, 2n-1$.

$$C_c = \cos\left(\frac{4}{3}\pi\, n_{\downarrow}(S)\right)\operatorname{sign}\kappa' \tag{38}$$

$$\mathcal{S}_c = -\sin\left(\frac{4}{3}\pi\, n_{\downarrow}(S)\right) \tag{39}$$

$$\mathcal{S}_s = \sin\left(\frac{4}{3}\pi\, n_{\downarrow}(S)\right)\operatorname{sign}\kappa' \tag{40}$$

$$C_s = \cos\left(\frac{4}{3}\pi\, n_{\downarrow}(S)\right) \tag{41}$$

Therefore, let us focus, on the following integral, which we can integrate by parts:

$$\int_0^{\kappa} C_c\,\frac{\cos\left(\frac{4}{3}\ \arcsin\kappa^{3/2}\right)}{\sqrt{\kappa}\ \sqrt{1-\kappa^3}}\,\mathrm{d}\kappa = C_c\,\mathbb{C}(\kappa) - \mathbb{C}(1)\ \sum_{n_{\downarrow}} \Delta C_c \tag{42}$$

where ΔC_c are the values of the jumps every time κ' changes sign from positive to negative and

$$\mathbb{C}(\kappa) = \int_0^{\kappa} \frac{\cos\left(\frac{4}{3}\ \arcsin\kappa^{3/2}\right)}{\sqrt{\kappa}\ \sqrt{1-\kappa^3}}\,\mathrm{d}\kappa = 2\ \sqrt{\kappa}\,\cos\left(\frac{1}{4}\beta(\kappa)\right) \tag{43}$$

where the integral in equation (43) can be solved by the change of variables $Z = 4/3\ \arcsin\kappa^{3/2}$. Similarly,

$$\mathbb{S}(\kappa) = \int_0^{\kappa} \frac{\sin\left(\frac{4}{3}\ \arcsin\kappa^{3/2}\right)}{\sqrt{\kappa}\ \sqrt{1-\kappa^3}}\,\mathrm{d}\kappa = 2\ \sqrt{\kappa}\,\sin\left(\frac{1}{4}\beta(\kappa)\right) \tag{44}$$

In summary

$$\begin{aligned} x(\bar{S}) &= \tfrac{1}{S_{\max}^{*}} - I_{c_\theta}(\kappa_1) + I_{c_\theta}(\kappa) \\ y(\bar{S}) &= -I_{s_\theta}(\kappa_1) + I_{s_\theta}(\kappa) \end{aligned} \tag{45}$$

with

$$I_{c_\theta}(\kappa) = \cos\beta_1\, I_{c_\beta}(\kappa) + \sin\beta_1\, I_{s_\beta}(\kappa) \tag{46}$$

$$I_{s_\theta}(\kappa) = \sin\beta_1\, I_{c_\beta}(\kappa) - \cos\beta_1\, I_{s_\beta}(\kappa) \tag{47}$$

with $\kappa_1 = \kappa(1/S_{\max}{}^*)$ and

$$I_{c_\beta} = \frac{1}{2\,\alpha}\left[C_c\,\mathbb{C}(\kappa) + \mathcal{S}_c\,\mathbb{S}(\kappa) - \mathbb{C}(1)\sum_{n_\downarrow}\Delta C_c - \mathbb{S}(1)\sum_{n_\downarrow}\Delta\mathcal{S}_c\right] \tag{48}$$

$$I_{s_\beta} = \frac{1}{2\,\alpha}\left[\mathcal{S}_s\,\mathbb{C}(\kappa) - C_s\,\mathbb{S}(\kappa) - \mathbb{C}(1)\sum_{n_\downarrow}\Delta\mathcal{S}_s + \mathbb{S}(1)\sum_{n_\downarrow}\Delta C_s\right] \tag{49}$$

4. Results

We have compared the analytical derivation with the numerical solution of the ODE in equation (12). The analytical solution is obtained through solving the nonlinear equation (23) with the function fzero in Matlab. In figures 8, we consider dimensionless loads $q_n{}^*$ such that $1/S_{\max}{}^*$ is an integer

$$q_n{}^* = q_1{}^*\, n^3 = \left(2\;{}_2F_1\left(\frac{1}{6},\frac{1}{2};\frac{7}{6},1\right)\right)^3 n^3 \approx 14.325\, n^3 \tag{50}$$

where $q_1{}^*$ is the load such that $1/S_{\max}{}^* = 1$. The analytical and numerical curves overlap, reassuring us of the exactness of the analytical solutions. Figures 8a-f display intriguing features of the deformation. When $n = 2$ (figure 8b), $S^* = 2$ is equal to a full period of the solution. For such load, the rod deforms into a drop-like loop. This shape is akin to the one obtained numerically by Faulkner et al. (1993). Also, this occurrence is similar to the self-encapsulating of the elastica as reported experimentally in Bosi et al. (2015).

The number of drops increases to 2 when $n = 4$ (figure 8d) and to 3 when $n = 6$ (figure 8f). This trefoil shape appears to be a Kiepert curve (Wegner, 2019). Such curve is a buckled ring solution identified by Greenhill (1899). Interestingly, we find this solution when the initial configuration is a straight rod; Greenhill (1899) obtained the Kiepert curve as a buckling solution when the initial configuration is a circumference.

One would then wonder if the loops increase to 4 when $n = 8$. Interestingly, they do not. Figures 9a-e show that for loads greater than $q_6{}^*$, the loops remain three, with the rod overlapping onto itself. The radius of the loops decreases, since $x/L, y/L \sim (q^*)^{-1/3}$, while rotating around the origin.

5. Conclusion

We presented the analytical solution of the cantilevered elastica under a uniformly distributed follower load. We derive curvature, rotation and deformation in Cartesian coordinates. The curvature is the solution of an autonomous undamped Duffing equation with a constant forcing term. For this case, the solution is a periodic function given in implicit form. A change of variables allows the integration of the curvature, to obtain rotation and deformations.

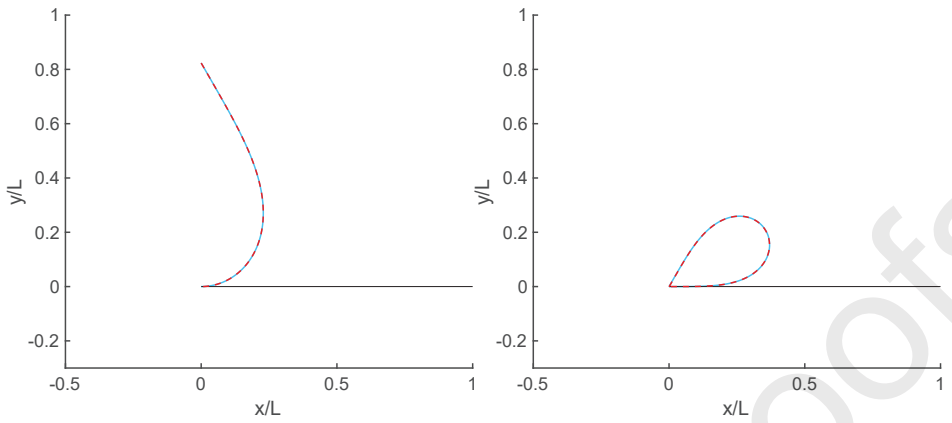

(a) $n = 1,\ q_1^* = 14.325$

(b) $n = 2,\ q_2^* = 114.600$

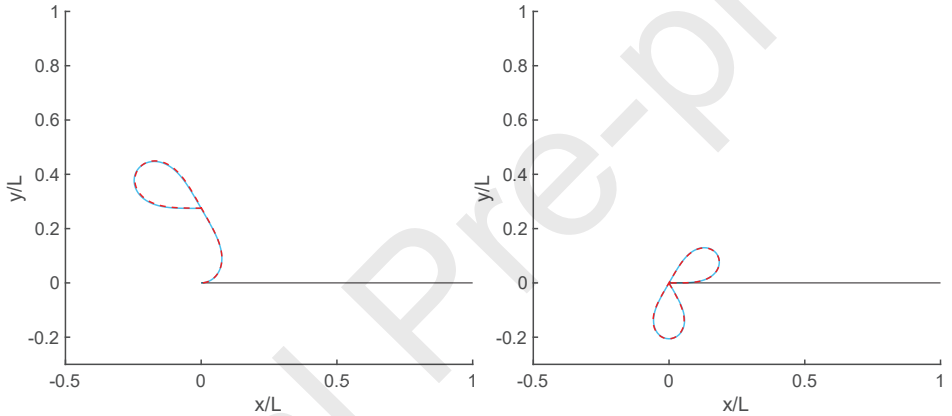

(c) $n = 3,\ q_3^* = 386.775$

(d) $n = 4,\ q_4^* = 916.800$

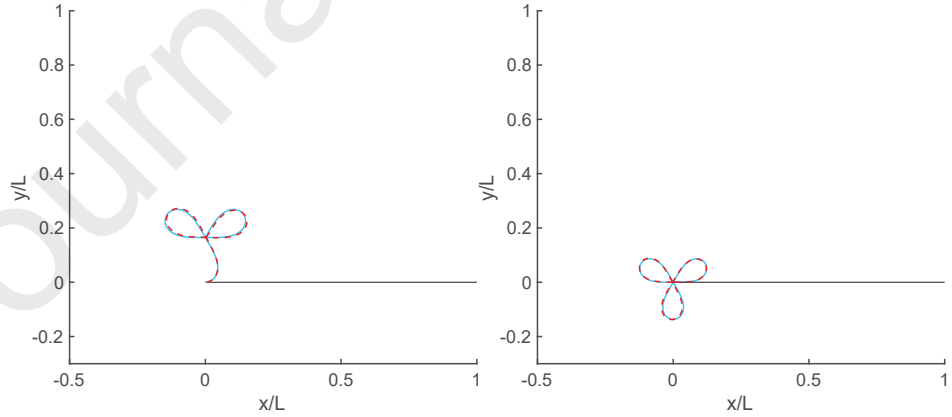

(e) $n = 5,\ q_5^* = 1790.6$

(f) $n = 6,\ q_6^* = 3094.2$

Figure 8: Deformation of the elastica, with x and y being the dimensional Cartesian coordinates. Black line: $q^* = 0$, blue continuous lines are the analytical solutions, red dashed lines are the numerical solutions. q_n^* as in equation (50). No self-contact constraint is imposed.

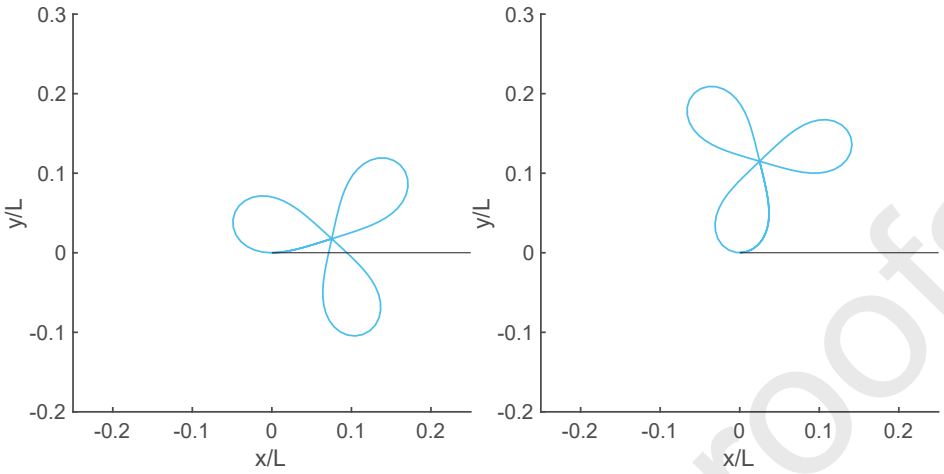

(a) $q* = 3942.2$ (b) $q^* = 4790.3$

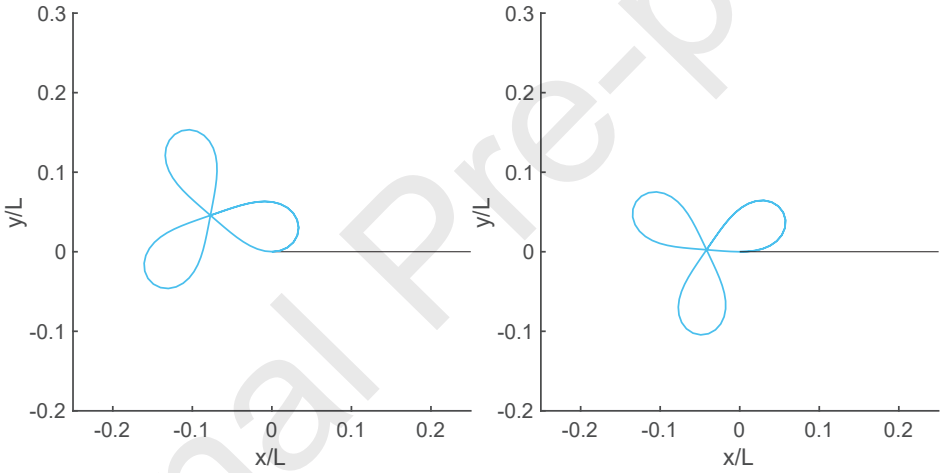

(c) $q^* = 5638.3$ (d) $q^* = 6486.4$

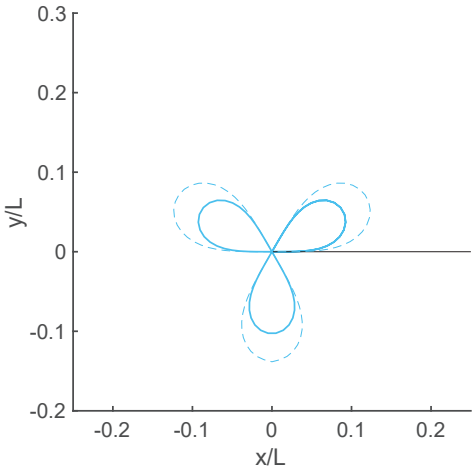

(e) $q^* = 7334.4$ (dashed line $q^* = q_6{}^* = 3094.2$)

Figure 9: Deformation of the elastica, with x and y being the dimensional Cartesian coordinates. Black line: $q^* = 0$, blue continuous lines are the analytical solutions. No self-contact constraint is imposed.

6. Acknowledgments

The author would like to thank Prof Davide Bigoni from the University of Trento, Italy, for his useful comments on the elastica subjected to follower loads and for his encouragement to write this paper. The author is grateful to Dr Diego Misseroni for the fruitful discussions. The author also thanks the anonymous reviewers for their constructive criticisms and for pointing out the similarities with the Kiepert curve.

The MATLAB code for all the calculations is available from the MATLAB File Exchange at https://jp.mathworks.com/matlabcentral/fileexchange/74373-euler-s-elastica-follower-load.

Antman, S., 1968. General solutions for plane extensible elasticae having nonlinear stress-strain laws. Quarterly of Applied Mathematics 26 (1), 35–47.

Antman, S. S., 1995. Nonlinear Problems of Elasticity. Springer.

Batista, M., 2014. Analytical treatment of equilibrium configurations of cantilever under terminal loads using Jacobi elliptical functions. International Journal of Solids and Structures 51 (13), 2308–2326.

Beck, M., 1952. The buckling load of the unilaterally clamped, tangentially pressed rod. Journal of Applied Mathematics and Physics ZAMP 3 (3), 225–228.

Bigoni, D., 2012. Nonlinear Solid Mechanics: Bifurcation Theory and Material Instability. Cambridge University Press.

Bigoni, D., Kirillov, O. N., Misseroni, D., Noselli, G., Tommasini, M., 2018a. Flutter and divergence instability in the Pflüger column: Experimental evidence of the ziegler destabilization paradox. Journal of the Mechanics and Physics of Solids 116, 99–116.

Bigoni, D., Misseroni, D., 2020. Structures loaded with a force acting along a fixed straight line, or the "Reut's column problem". Journal of the Mechanics and Physics of Solids 134, 103741.

Bigoni, D., Misseroni, D., Tommasini, M., Kirillov, O. N., Noselli, G., 2018b. Detecting singular weak-dissipation limit for flutter onset in reversible systems. Physical Review E 97 (2), 023003.

Bigoni, D., Noselli, G., 2011. Experimental evidence of flutter and divergence instabilities induced by dry friction. Journal of the Mechanics and Physics of Solids 59 (10), 2208–2226.

Bolotin, V. V., 1963. Nonconservative Problems of the Theory of Elastic Stability. Macmillan.

Bosi, F., Misseroni, D., Dal Corso, F., Bigoni, D., 2015. Self-encapsulation, or the 'dripping'of an elastic rod. Proceedings of the Royal Society A: Mathematical, Physical and Engineering Sciences 471 (2179), 20150195.

Bottema, O., 1956. The Routh-Hurwitz condition for the biquadratic equation. Indagationes Mathematicae 18, 403–406.

Djondjorov, P. A., Vassilev, V. M., Mladenov, I. M., 2011. Analytic description and explicit parametrisation of the equilibrium shapes of elastic rings and tubes under uniform hydrostatic pressure. International Journal of Mechanical Sciences 53 (5), 355–364.

Elishakoff, I., 2005. Controversy associated with the so-called "follower forces": critical overview. Applied Mechanics Reviews 58 (2), 117–142.

Faulkner, M. G., Lipsett, A. W., Tam, V., 1993. On the use of a segmental shooting technique for multiple solutions of planar elastica problems. Computer Methods in Applied Mechanics and Engineering 110 (3-4), 221–236.

Frisch-Fay, R., 1962. Flexible Bars. Butterworths.

Fujii, F., Naito, M., Gong, S.-X., 1990. Finite displacement theory of straight beams under configuration-dependent uniform loads. Computers & Structures 36 (1), 157–167.

Giomi, L., 2013. Softly constrained films. Soft Matter 9 (34), 8121–8139.

Giomi, L., Mahadevan, L., 2012. Minimal surfaces bounded by elastic lines. Proceedings of the Royal Society A: Mathematical, Physical and Engineering Sciences 468 (2143), 1851–1864.

Greenhill, A., 1899. The elastic curve, under uniform normal pressure. Mathematische Annalen 52 (4), 465–500.

Herrmann, G., Nemat-Nasser, S., Prasad, S., 1966. Models demonstrating instability of non-conservative mechanical systems. Northwestern University Structural Mechanics Laboratory Technical Report 66-4.

Iandiorio, C., Salvini, P., 2020. Large displacements of slender beams in plane: Analytical solution by means of a new hypergeometric function. International Journal of Solids and Structures 185, 467–484.

Lévy, M., 1884. Memoire sur un nouveau cas integrable du probleme de l'elastique et l'une des ses applications. Journal de Mathématiques Pures et Appliquées 10, 5–42.

Manning, R. S., 2014. A catalogue of stable equilibria of planar extensible or inextensible elastic rods for all possible Dirichlet boundary conditions. Journal of Elasticity 115 (2), 105–130.

Mitchell, T. P., 1959. The nonlinear bending of thin rods. Journal of Applied Mechanics 26, 40–43.

Mora, S., Phou, T., Fromental, J.-M., Audoly, B., Pomeau, Y., 2012. Shape of an elastic loop strongly bent by surface tension: Experiments and comparison with theory. Physical Review E 86 (2), 026119.

Pflüger, A., 1950. Stabilitätsprobleme der Elastostatik. Springer-Verlag.

Pflüger, A., 1955. To stabilize the tangential bar. ZAMM Journal of Applied Mathematics and Mechanics 35 (5), 191–191.

Reut, V., 1939. About the theory of elastic stability. Proceedings of the Odessa Institute of Civil and Communal Engineering 1, 126–138.

Salussolia, G., Barbieri, E., Pugno, N. M., Botto, L., 2020. Micromechanics of liquid-phase exfoliation of a layered 2d material: A hydrodynamic peeling model. Journal of the Mechanics and Physics of Solids 134, 103764.

Scarpello, G. M., Ritelli, D., 2011. Exact solutions of nonlinear equation of rod deflections involving the lauricella hypergeometric functions. International Journal of Mathematics and Mathematical Sciences 2011.

Sugiyama, Y., Katayama, K., Kinoi, S., 1995. Flutter of cantilevered column under rocket thrust. Journal of Aerospace Engineering 8 (1), 9–15.

Sugiyama, Y., Katayama, K., Kiriyama, K., Ryu, B.-J., 2000. Experimental verification of dynamic stability of vertical cantilevered columns subjected to a sub-tangential force. Journal of Sound and Vibration 236 (2), 193–207.

Sugiyama, Y., Langthjem, M., Ryu, B., 1999. Realistic follower forces. Journal of Sound and Vibration 225 (4), 779–782.

Tommasini, M., Kirillov, O. N., Misseroni, D., Bigoni, D., 2016. The destabilizing effect of external damping: Singular flutter boundary for the pflüger column with vanishing external dissipation. Journal of the Mechanics and Physics of Solids 91, 204–215.

Truesdell, C., 1953. A new chapter in the theory of the elastica. In: Proceedings of the 1st Midwestern Conference on Solid Mechanics. pp. 52–55.

Vassilev, V., Djondjorov, P. A., Mladenov, I., 2008. Cylindrical equilibrium shapes of fluid membranes. Journal of Physics A: Mathematical and Theoretical 41 (43), 435201.

Wegner, F., 2019. From elastica to floating bodies of equilibrium. arXiv preprint arXiv:1909.12596v4.

Wood, W., Saw, S., Saunders, P., 1969. The kinetic stability of a tangentially loaded strut. Proceedings of the Royal Society of London. A. Mathematical and Physical Sciences 313 (1513), 239–248.

Ziegler, H., 1952. Die stabilitätskriterien der elastomechanik. Archive of Applied Mechanics 20 (1), 49–56.

Ziegler, H., 1956. On the concept of elastic stability. In: Advances in Applied Mechanics. Vol. 4. Elsevier, pp. 351–403.

Ziegler, H., 1977. Principles of Structural Stability. Vol. 35. Birkhäuser.